(Received 19 March 2026, Accepted 22 April 2026, Scheduled 14 May 2026)

EMI Filter Parameter Design Optimization Based on Improved Particle Swarm Algorithm

Jian Zheng[1], Fang Liu[1], Shuangyin Cheng[2,*], Zhenwei Zhang[1], and Zhijie Chen[1]

[1] College of Electrical and Information Engineering, Hunan University of Technology, Zhuzhou 412007, China
[2] Changsha NM Drive Technology Co., Ltd, Changsha 410205, China

ABSTRACT: When designing the parameters of electromagnetic interference filters in BUCK rectifiers using a particle swarm optimization algorithm, the resulting solution set tends to fall into local optima, resulting in a lower cost-performance ratio for the filters. Therefore, an optimization scheme for the parameter design is proposed. First, a multi-objective optimization model is established, with common-mode capacitance and inductance, as well as differential-mode capacitance as decision variables, conducted noise and cost as the objective function, and conducted noise limits and leakage current as constraints. Next, three improvements are made to the conventional algorithm, classifying initialization for the particle population, dividing the total number of iterations into stages with differentiated handling, and implementing an adaptive early termination for iterations, thereby an improved algorithm is obtained. Finally, both the improved and conventional algorithms are applied to solve the optimization model, yielding two types of optimal solutions: performance-prioritized and cost-prioritized solutions. The comparison results show that, between the two optimal solutions, the performance of the improved algorithm is similar to that of the conventional algorithm, but its cost is reduced by 28.37% and 53.14%, respectively. Meanwhile, the Pareto solution set obtained by the improved algorithm is more widely distributed, avoiding local optima, and the iterative convergence efficiency of the improved algorithm was improved by 81%.

1. INTRODUCTION

Buck-type rectifiers are widely used in medium and small power converters. However, the negative impact of electromagnetic interference (EMI) generated by their high-frequency switching characteristics on the system cannot be ignored. Adding a passive filter at the output port of an AC power supply is a common solution for suppressing EMI [1–3]. After the circuit structure of the EMI filter is determined, the design of its component parameters must comprehensively consider the insertion loss, volume, cost, and safety regulations requirements, which is a typical multi-objective optimization problem [4]. Therefore, optimizing the design of the component parameters is a key to improving the performance and reducing the cost of EMI filters [5].

Most conventional methods for EMI filter parameter design are based on engineering experience or analytical calculations of simplified models. Ref. [6] calculated the component parameters based on the traditional design process using empirical formulas. Ref. [7] established a high-frequency equivalent model for the EMI filter of an onboard DC-DC converter and derived parameter constraints, with core parameters still determined through analytical calculations and manual verification. Ref. [8] investigated the design of EMI filters under parasitic coupling and the optimal arrangement of components, where parameters such as inductance and capacitance were manually adjusted based on engineering experience combined with simulation iterations. The above-mentioned studies did not automatically optimize the component parameters and had a long design cycle. At high frequencies, volume redundancy or insufficient insertion loss is prone to occur [9].

Intelligent algorithms have been introduced into the parameter design of EMI filters to achieve automatic optimization of component parameters. Ref. [10] adopted an improved differential evolution algorithm to optimize the insertion loss of the filter. Its adaptive mechanism enhanced the quality of a solution set, but the parameter adjustment was rather complex. Ref. [11] adopted an improved differential evolution algorithm to optimize the insertion loss of a filter. Its adaptive mechanism enhanced the quality of the solution set, but the parameter adjustment was rather complex. Ref. [12] compared the genetic algorithm with the particle swarm optimization (PSO) algorithm and concluded that the PSO algorithm converged faster in parameter optimization, had a simpler structure, and required fewer adjustment parameters. At present, the PSO algorithm is widely used in the parameter design of power filters, but is relatively less used in the parameter design of EMI filters. Ref. [13] optimized the parameters of EMI filters by converting multiple targets into single-target processing using "weighted summation". The optimized solution depends on the prior selection of weight coefficients and can only provide a single solution. The multi-objective PSO (MOPSO) algorithm can directly output multiple optimal solutions and has attracted the attention of many researchers [14, 15]. Refs. [16, 17] improved the MOPSO algorithm to enhance the quality, diversity, and convergence of the solution set.

* Corresponding author: Shuangyin Cheng (liam.cheng@nmdrive.cn).

Based on the above studies, we applied the MOPSO algorithm to the parameter design of EMI filters for BUCK-type rectifiers and found that the obtained solution set was prone to fall into the high-cost region, resulting in a low cost performance of the filter. Therefore, in this study, an optimization scheme for parameter design is proposed. First, a multi-objective optimization model was established for the parameters. The conventional MOPSO algorithm was then improved to obtain an improved algorithm. Finally, the improved and conventional algorithms were applied to solve the optimization model, and their results were compared.

2. OPTIMIZATION MODELING OF EMI FILTER PARAMETERS

2.1. Conducted Noise of BUCK Rectifier

The BUCK-type rectifier is shown in Fig. 1(a). Its main structure is "single-phase mains power + diode full-bridge rectification + BUCK converter", with a switching frequency of 100 kHz, an output DC voltage of 20 V, and an output power of 250 W. The conducted noise spectrum measured by the Linear Impedance Stabilization network (LISN) is shown in Fig. 1(b). In Fig. 1(b), the common-mode noise N_{CM}, differential-mode noise N_{DM}, and EMI noise N_{EMI} are all the peak values, and the standard limit N_{base} is the quasi-peak value [18]. It can be seen from Fig. 1(b) that all three types of noise significantly exceed the standard limit. From this, it can be inferred that the quasi-peak values corresponding to the three types of noise would exceed the standard limit. Within the measured frequency band, the lowest frequency with the highest noise of common mode (NCM) and noise of differential mode (NDM) that exceed the Nbase occurs at 200 kHz. At this frequency, the three noise peaks are 92.2 dBμV, 87.8 dBμV, and 80 dBμV, respectively,

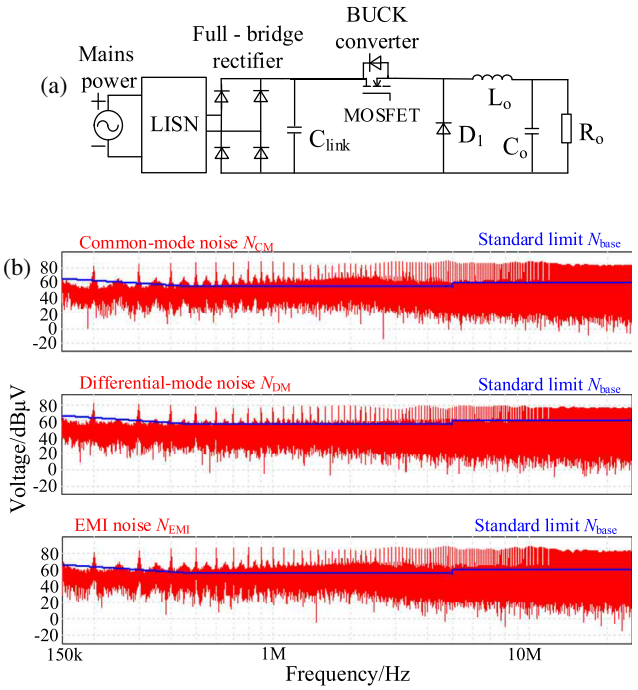

FIGURE 1. BUCK rectifier with EMI filter inserted.

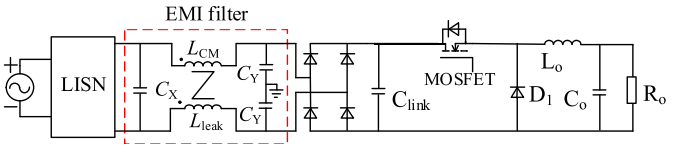

FIGURE 2. BUCK rectifier with EMI filter inserted.

while the corresponding standard limit is 63.6 dBμV. Therefore, it is necessary to suppress these noises. One of the most effective means is to add an EMI passive filter at the output port of the AC power supply. For medium and small power converters, the filter circuit generally adopts an L-shaped two-stage structure, as shown in Fig. 2. In Fig. 2, C_X, C_Y, L_{CM}, and L_{leak} represent the inductance and leakage inductance of the differential-mode capacitor, common-mode capacitor, and common-mode choke, respectively.

2.2. Multi-Objective Optimization Modeling of EMI Filter Parameters

After the circuit structure of the EMI filter is determined, the design of its component parameters is vital. Parameter design is a typical multi-objective optimization problem. In this study, C_X, C_Y and L_{CM} are selected as decision variables $\mathbf{x}$, which are expressed as

$$\mathbf{x} = [C_X, C_Y, L_{\mathrm{CM}}]^{\mathrm{T}} \tag{1}$$

In the decision variables, the differential mode inductance is not directly considered because the differential mode filtering function can be achieved through common mode leakage inductance. Generally, the common mode leakage inductance $L_{\mathrm{leak}} = 0.05 L_{\mathrm{CM}}$. Therefore, only L_{CM} is considered for the inductance, which can achieve a low-cost effect.

This study aims to minimize the noise and cost functions of the system while satisfying electromagnetic compatibility standards and safety regulations. The optimization model is calculated as follows

$$\begin{cases} \min & \mathbf{F}(\mathbf{x}) = [F_1(\mathbf{x}), F_2(\mathbf{x})]^{\mathrm{T}} \\ \text{s.t.} & g_j(\mathbf{x}) \le 0, \quad j = 1, 2 \end{cases} \tag{2}$$

where $F_1(\mathbf{x})$ is the noise function, and $F_2(\mathbf{x})$ is the cost function.

The expression of the noise function $F_1(\mathbf{x})$ is as follows

$$F_1(\mathbf{x}) = \sum_{j=1}^{m} \left\{ w_j \cdot \max \left[N'_{\mathrm{CM}j}(f_j), N'_{\mathrm{DM}j}(f_j) \right] \right\} \tag{3}$$

where $N'_{\mathrm{CM}j}(f_j)$ and $N'_{\mathrm{DM}j}(f_j)$ are the predicted values of the filtered common-mode and differential-mode noises after filtering, respectively; m is the total number of sampling points within the frequency band; w_j is the weighting coefficient for the jth frequency point, which is set according to the degree of exceedance of the common-mode and differential-mode noise limits, and satisfies $\sum_{j}^{m} w_j = 1$.

The calculation formula for the weighting coefficient w_j is

$$w_j = \frac{\Delta N(f_j)}{\sum_{i=1}^{m} \Delta N(f_i)} \tag{4}$$

where the calculation formula for $\Delta N(f_j)$ is

$$\Delta N(f_j) = \max\left[N'_{\mathrm{CM}j}(f_j), N'_{\mathrm{DM}j}(f_j)\right] - N_{\mathrm{base}}(f_j) \tag{5}$$

The predicted values of the common-mode and differential-mode noises after filtering were calculated as follows:

$$N'_{\mathrm{CM}}(f) = [N_{\mathrm{CM}}(f) - \Delta] - IL_{\mathrm{CM}}(f) \tag{6}$$

$$N'_{\mathrm{DM}}(f) = [N_{\mathrm{DM}}(f) - \Delta] - IL_{\mathrm{DM}}(f) \tag{7}$$

In the formula, Δ is the design margin, which is taken as 6 dBμV here to avoid the risk of weighting coefficients causing bias at specific frequency points; $IL_{\mathrm{CM}}(f)$ and $IL_{\mathrm{DM}}(f)$ are the common-mode and differential-mode insertion losses, respectively.

The insertion losses were calculated based on the second-order filter theory, considering the parasitic parameters of the filter, which are expressed as

$$IL'_{\mathrm{CM}}(f) = 20\lg\left|\frac{Z_S(f) + Z_{\mathrm{CM}}(f)}{Z_L(f) + Z_{\mathrm{CM}}(f)}\right| \tag{8}$$

$$IL'_{\mathrm{DM}}(f) = 20\lg\left|\frac{Z_S(f) + Z_{\mathrm{DM}}(f)}{Z_L(f) + Z_{\mathrm{DM}}(f)}\right| \tag{9}$$

where Z_s is the noise source impedance; Z_L is the impedance on the power supply side; and Z_{CM} and Z_{DM} are the common-mode and differential-mode impedances, respectively.

The expression of the cost function $F_2(\mathbf{x})$ is as follows

$$F_2(x) = h_1\left(\frac{C_X}{C_{X0}}\right)^{\alpha} + h_2\left(\frac{C_Y}{C_{Y0}}\right)^{\beta} + h_3\left(\frac{L_{\mathrm{CM}}}{L_{\mathrm{CM0}}}\right)^{\gamma} \tag{10}$$

where h_1, h_2, and h_3 are cost coefficients, reflecting the relative cost impacts of X capacitors, Y capacitors, and common-mode chokes, with values of 0.15, 0.25, and 0.5, respectively. The scale indices α, β, and γ characterize the sublinear growth characteristics of component costs, with values of 0.8, 0.7, and 0.7, respectively. C_{X0}, C_{Y0}, and L_{CM0} are the baseline values for dimensionless quantification, typically representing the characteristic orders of magnitude within the parameter range of the components. For a 250 W BUCK-type rectifier's EMI filter, the values are taken as 1 μF, 1 nF, and 1 mH, respectively.

There are two constraints subject to electromagnetic compatibility (EMC) standards and safety requirements: The first constraint is that the noise function is less than the standard limit, which is expressed as follows

$$g_1(\mathbf{x}) = F_1(\mathbf{x}) - N_{\mathrm{base}} \le 0 \tag{11}$$

The second constraint $g_2(\mathbf{x})$ is that the ground leakage current is less than the maximum allowable leakage current specified in IEC60335.1, that is

$$g_2(\mathbf{x}) = I_{\mathrm{leak}}(\mathbf{x}) - I_{\max} \le 0 \tag{12}$$

where I_{leak} is the leakage current to the ground, and $I_{\max}$ is the maximum allowable leakage current, which is 3.5 mA.

The calculation formula for the leakage current to ground is

$$I_{\mathrm{leak}}(\mathbf{x}) = 2\pi V_{\mathrm{rms}} f_{\mathrm{line}} C_Y \tag{13}$$

where V_{rms} is the effective value of the AC power supply, and f_{line} is the line frequency. This formula takes into account the variation of f_{line} and the tolerance of C_Y.

The ranges of the decision variables are determined according to engineering practice, component supply, and safety specifications. In the EMI filter of a 250 W BUCK-type rectifier, the typical range of values is as follows

$$0.1\,\mu\mathrm{F} \le C_X \le 4.7\,\mu\mathrm{F} \tag{14}$$

$$0.1\,\mathrm{nF} \le C_Y \le 4.7\,\mathrm{nF} \tag{15}$$

$$0.1\,\mathrm{mH} \le L_{\mathrm{CM}} \le 3.0\,\mathrm{mH} \tag{16}$$

3. IMPROVED PARTICLE SWARM OPTIMIZATION ALGORITHM

The MOPSO algorithm is one of the most effective methods for solving the above-mentioned optimization model. The conventional MOPSO algorithm has certain limitations when solving the parameter optimization of EMI filters. It may fall into a local optimum during the search process, and the obtained solution set has further room for improvement in terms of distribution and convergence. Therefore, this study makes three improvements to the conventional MOPSO. First, the initialization of the particle swarm is performed by classified initialization to add potential high-quality solutions while ensuring the diversity of the particle population. Second, the total number of iterations is divided into two stages to provide empirical value guidance for the particle swarm search to avoid blind exploration. Third, adaptive early termination is implemented for the number of iterations to enhance the convergence efficiency while ensuring the quality of the solution set. Fig. 3 shows the flowchart of the improved algorithm.

3.1. Initialization of Particle Population Classification

The first shaded box in Fig. 3 reflects this improvement. Unlike the conventional MOPSO algorithm, the improved algorithm does not generate particles randomly. Instead, it generates two types of particles. The first type is experience-guided particles, and the second type is randomly selected exploratory particles. The specific proportions of the two types of particles were determined by the parameter sensitivity analysis of the algorithm.

First, the first type of particles is generated by small-range random perturbations near the empirical high-quality solutions, enabling the algorithm to focus on the high-quality solution regions guided by engineering experience in the initial stage. The range formula is as follows

$$\mathbf{x}_i^{(0)} = \mathbf{x}_{\mathrm{guide}}(1 + \boldsymbol{\delta}) \tag{17}$$

where $\mathbf{x}_i^{(0)}$ represents the position of the ith particle at the 0th iteration (i.e., the initialization), and $\mathbf{x}_{\mathrm{guide}}$ is the particle position determined by an experience-guided value, which is referred to

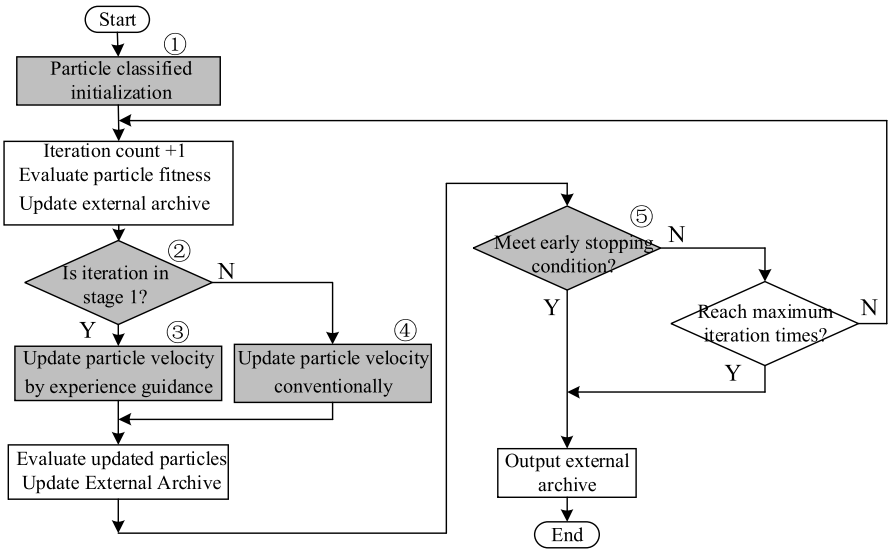

FIGURE 3. Flowchart of the improved MOPSO algorithm.

in this paper as the empirical high-quality solution. For example, in the EMI filter of a 250 W BUCK-type rectifier, according to (14)–(16), $\mathbf{x}_{\text{guide}}$ can take the values [2.2, 2.2, 1.5]. δ is a perturbation vector whose components are independent and follow a uniform distribution on $[-0.3, 0.3]$.

Then, within the full feasible range of parameters, the second type of particle was randomly generated in the usual way to ensure the diversity of the particle population.

3.2. Phased Processing of the Total Number of Iterations

The second to fourth shaded boxes in Fig. 3 reflect this improvement. Unlike the conventional MOPSO algorithm, the total number of particle iterations in the improved algorithm was divided into two stages. The initial iterations are assigned to the first stage, whereas the remaining iterations are assigned to the second stage. The specific proportion of iterations for the two stages was determined by the parameter sensitivity analysis of the algorithm.

In the iteration times of the first stage, the velocity update equation of all particles added an experience-guided term, whereas in the iteration times of the second stage, the velocity update equation of all particles followed the conventional equation.

In the conventional MOPSO algorithm, the update equations for the $\mathbf{v}_i$ and position $\mathbf{x}_i$ of particle i in each iteration are as follows

$$\mathbf{v}_i^{k+1} = w^k \mathbf{v}_i^k + c_1 r_1 (\mathbf{p}_i^k - \mathbf{x}_i^k) + c_2 r_2 (\mathbf{g}^k - \mathbf{x}_i^k) \quad (18)$$

$$\mathbf{x}_i^{k+1} = \mathbf{x}_i^k + \mathbf{v}_i^{k+1} \quad (19)$$

where k is the number of iterations in the algorithm; c_1 and c_2 are acceleration coefficients that adjust the maximum step size of flight toward the individual historical best and global best, respectively; r_1 and r_2 are random numbers with values in the range [0, 1]; $\mathbf{p}_i$ is the historical best solution for individual particle i; $\mathbf{g}$ is the historical best solution for the particle swarm; w is the inertia weight coefficient, which reflects the degree to which the particle maintains its current velocity. The calculation formula is as follows

$$w^k = w_{\max} - \frac{k}{K}(w_{\max} - w_{\min}) \quad (20)$$

where $w_{\max}$ and $w_{\min}$ are the maximum and minimum values of the inertia weight coefficient, respectively; k and K are the current and total iteration numbers, respectively.

To accelerate the algorithm convergence and guide the particles toward better design regions, an empirical guidance term is introduced into Equation (16) during the first-stage iterations in this study, and the result is as follows

$$\mathbf{v}_i^{k+1} = \omega^k \mathbf{v}_i^k + c_1 r_1 \left(\mathbf{p}_i^k - \mathbf{x}_i^k\right) + c_2 r_2 \left(\mathbf{g}^k - \mathbf{x}_i^k\right) + c_3^k r_3 \left(\mathbf{x}_{\text{guide}} - \mathbf{x}_i^k\right) \quad (21)$$

where c_3 is the experiential learning factor, used to adjust the step size of the particle moving in the direction of prior experience. The range of values for random number r_3 is the same as r_1 and r_2.

The value of the empirical learning factor c_3 is the key to balancing the utilization of prior knowledge and the ability to independently explore. If c_3 remains constant, the algorithm might still be excessively restricted by prior experience in the later iteration stage, thereby inhibiting its ability to escape local optima and conduct fine search. Therefore, in this study, an adaptive attenuation strategy is introduced to make c_3 vary dynamically with the number of iterations. Its value decays exponentially from the initial strength to adjust the weight of the empirical guidance. The calculation formula is as follows

$$c_3^k = c_3^{(0)} \cdot \exp\left(-\lambda \frac{k}{K}\right) \quad (22)$$

where c_3^k is the empirical learning factor at the kth iteration, $c_3^{(0)}$ the initial value at the 0th iteration, and λ the decay coefficient.

TABLE 1. Comparison between conventional MOPSO and improved MOPSO.

	Conventional MOPSO	Improved MOPSO
Population initialization	Particles are generated purely through a random process.	Particles are categorized into experience-guided particles and random exploration particles.
Iteration strategy	The velocity update equation remains standard throughout all iterations.	In the initial stage, an experience-guided term is added to the velocity update equation. The remaining iterations follow the conventional equation.
Termination mechanism	Iterations continue until the maximum iteration limit is reached.	Iterations terminate early when three specific adaptive conditions are simultaneously met.

3.3. Adaptive Early Termination Mechanism for Iterations

The fifth shaded box in Fig. 3 illustrates the third improvement step. Unlike the conventional MOPSO algorithm, the improved algorithm does not always iterate the maximum number of times. Instead, it monitors the changes in the external archive over several consecutive iterations and terminates the iteration process early when the preset conditions are met, effectively reducing the computational cost.

Let S_k be the number of solutions in the external archive at the kth iteration. Considering five consecutive iterations before the kth iteration, the external archive size sequence S_{recent} is defined as

$$S_{\text{recent}} = \{S_{k-4}, S_{k-3}, S_{k-2}, S_{k-1}, S_k\} \tag{23}$$

The range ΔS of this sequence is

$$\Delta S = \max\left(S_{\text{recent}}\right) - \min\left(S_{\text{recent}}\right) \tag{24}$$

where a smaller ΔS indicates the better stability of the high-quality solution. When $\Delta S \leq 3$, and combined with the previous two conditions, it indicates that the solution sought has become stable.

The termination mechanism must satisfy three conditions simultaneously. The first condition is that the minimum number of iterations should be no less than 15 to ensure that the algorithm has a basic exploratory capability. The second condition is that S_k reaches more than 90% of the preset capacity to ensure the completeness of the solution set. The third condition is $\Delta S \leq 3$. When all three conditions were met simultaneously, the algorithm immediately terminated the iterations and outputted the external archive as the final optimization result.

4. RESULTS ANALYSES OF IMPROVED ALGORITHM

The improved algorithm above was applied to solve the optimization model in (2). The particle position $\mathbf{x}$ is defined as the decision variables $[C_X, C_Y, L_{\text{CM}}]^T$. The number of particles was set to 100, and the total number of iterations was set to 100. Through parameter sensitivity analyses of the algorithm, the best specific proportions of the two types of particles were determined to be 20% and 80%, and the best specific proportions of the two-stage iterations were determined to be 20% and 80%. After solving, a series of optimal solutions were obtained, from which two representative solutions were selected: the performance-priority solution and the cost-priority solution. To verify the effectiveness of the improved algorithm, the conventional algorithm was also used to solve the optimization model in (2), and the results are compared in Table 1.

As shown in Table 1, in the performance-prioritized solution, the improved algorithm significantly increases C_X while maintaining C_Y unchanged and reducing L_{CM}. From the perspective of insertion loss and impedance matching, increasing C_X can compensate for the reduction in L_{CM}. Through component parameter reconstruction, the noise function of the improved algorithm was comparable to that of the conventional algorithm, but the cost function was lower than that of the conventional algorithm, decreasing from the original 140.23 to 109.24, a reduction of 28.37%. The leakage currents of both algorithms are identical.

In the cost-priority solution, the improved algorithm simultaneously reduces C_X, C_Y, and L_{CM}. Through component parameter reconstruction, the noise function of the improved algorithm was slightly higher than that of the conventional algorithm, but the cost was significantly lower, decreasing from the original 94.21 to 61.52, a reduction of 53.14%, and the leakage current of the improved algorithm was lower than that of the conventional algorithm.

In addition, a vertical comparison between the performance-priority and cost-priority solutions of the improved algorithm revealed that the C_X, C_Y, and L_{CM} of the performance-prioritized solution were all greater than those of the cost-priority solution, achieving higher performance. However, the cost-priority solution significantly reduces the component parameters while still meeting the standards, resulting in lower costs. The two optimized solutions of the improved algorithm provide targeted approaches for different requirements.

The Pareto front plots of the two algorithms are shown in Figs. 4 and 5. As shown in Fig. 4, the solution set of the conventional algorithm exhibits a relatively concentrated distribution in the noise function — cost function objective plane, primarily clustered in high-cost regions. This indicates that the particles have a relatively limited exploration range and insufficient diversity. In contrast, as shown in Fig. 5, the solution set of the improved algorithm exhibits a wider distribution in the objec-

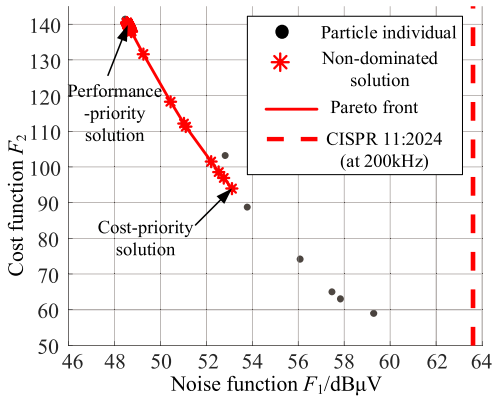

FIGURE 4. Pareto frontier plot of conventional algorithm.

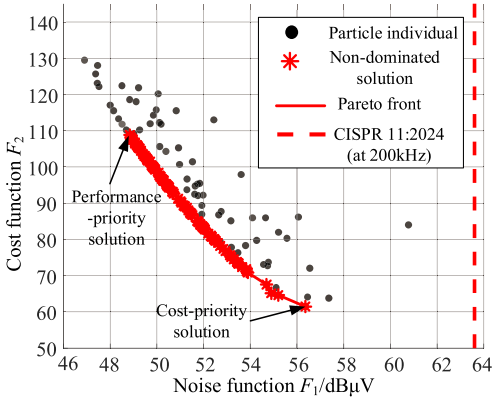

FIGURE 5. Pareto frontier plot of improved algorithm.

TABLE 2. Comparison of results between the two algorithms.

Two optimization solutions	Parameters and indicators	Conventional algorithm	Improved algorithm
Performance — Priority Solution	C_X	0.89 μF	3.51 μF
	C_Y	4.70 nF	4.70 nF
	L_{CM}	2.97 mH	2.05 mH
	$F_1(\mathbf{x})$	48.55 dBμV	48.81 dBμV
	$F_2(\mathbf{x})$	140.23	109.24
	I_{leak}	0.230 mA	0.230 mA
Cost — Priority Solution	C_X	1.84 μF	1.41 μF
	C_Y	4.70 nF	4.26 nF
	L_{CM}	1.66 mH	0.90 mH
	$F_1(\mathbf{x})$	53.12 dBμV	56.32 dBμV
	$F_2(\mathbf{x})$	94.21	61.52
	I_{leak}	0.230 mA	0.208 mA

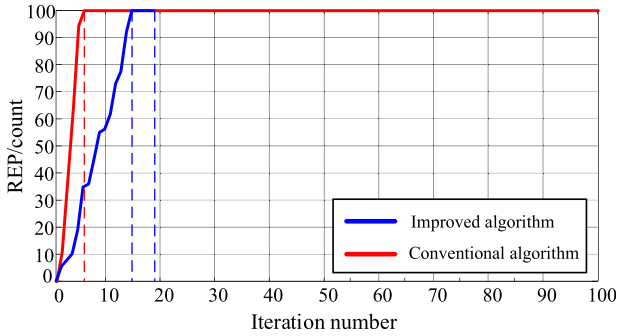

FIGURE 6. Final convergence history comparison of two algorithms.

tive plane, demonstrating significantly enhanced diversity and global exploration capabilities.

Figure 6 shows the final historical convergence graph of the two algorithms. As shown in Fig. 6, the actual total number of iterations for the conventional algorithm is 100, whereas for the improved algorithm it is only 19. This is because the improved algorithm incorporates an adaptive early termination mechanism that increases the convergence efficiency by 81%. Furthermore, Fig. 6 shows that the external archive curve of the conventional algorithm rises to saturation in the early iterations (approximately 4–6 generations) and then enters a plateau period, exhibiting typical premature convergence characteristics. This indicates that the solution set diversity of the algorithm sharply declines without fully exploring the solution space, making it prone to being trapped in local optima. In contrast, the external archive curve of the proposed algorithm grows slowly and steadily, gradually stabilizing around generations 14–16. This reflects that the algorithm continuously performs effective selection and evolution throughout the iterations, avoiding premature convergence and thus guiding the search toward high-quality solution regions in a stable and efficient manner.

The decision variables C_X, C_Y, and L_{CM} obtained from the improved algorithm in Table 2 were applied to the EMI filter shown in Fig. 2. The measured noise spectra are illustrated in Fig. 7, where N_{CM}, N_{DM}, and N_{EMI} represent the peak values, and the standard limit N_{base} is the quasi-peak value.

As shown in Fig. 7, the peak values of the conducted noise of the two optimized solutions do not exceed the standard within the measurement frequency band. Because the quasi-peak values are lower than the peak values, it can be inferred that the

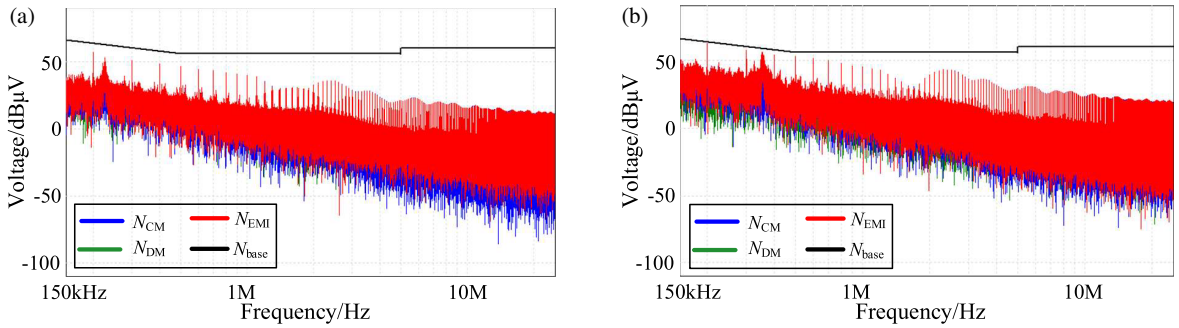

FIGURE 7. Conducted noise spectra of two optimization solutions for improved algorithm. (a) Performance-priority solution. (b) Cost-priority solution.

quasi-peak values of the conducted noise are far from exceeding the standard, further verifying that the improved algorithm is effective in optimizing the parameters of EMI filters.

5. CONCLUSION

This study focuses on the EMI filter parameter design of BUCK-type rectifiers. To address the limitations of the conventional MOPSO algorithm in EMI filter parameter design, such as insufficient solution set diversity, susceptibility to local optima, and excessive iterations, resulting in an EMI filter with a low cost-performance ratio, an optimized parameter design scheme is proposed. This scheme establishes a multi-objective optimization model for the parameters and introduces three improvements to the conventional MOPSO algorithm. Both the improved and conventional algorithms were applied to solve the optimization model. Comparative results demonstrate that the EMI filter parameters obtained using the improved algorithm achieve lower costs while meeting performance standards, resulting in a higher cost-performance ratio. The proposed scheme exhibits universality and can be extended to the parameter optimization design of EMI filters for other power converters.

ACKNOWLEDGEMENT

This work was supported by the National Natural Science Foundation of China (NSFC) under Grant 52477188 and Grant 62303178, and by the Natural Science Foundation of Hunan Province of China under Grant Number 2026JJ80067 and Grant 2025JJ80310.

REFERENCES

[1] Ruan, X., L. Xie, Q. Ji, and X. Yuan, *Conducted Electromagnetic Interference in Power Converters: Modeling, Prediction and Reduction*, Springer, 2024.

[2] Ma, Z., S. Wang, Q. Huang, and Y. Yang, "A review of radiated EMI research in power electronics systems," *IEEE Journal of Emerging and Selected Topics in Power Electronics*, Vol. 12, No. 1, 675–694, 2024.

[3] Hu, Y., X. Lei, X. Du, T. Ye, H. Song, and H. Li, "A review on high-frequency electromagnetic interference induced by power electronics in new electric power systems," *Global Energy Interconnection*, Vol. 8, No. 5, 804–820, 2025.

[4] Ozenbaugh, R. L., R. L. Pullen, and T. M. Pullen, *EMI Filter Design*, CRC Press, 2000.

[5] Zheng, J., C. Peng, L. Lin, and K. Zhao, "Common-mode voltage analyses for space vector PWM based on double Fourier series," *Progress In Electromagnetics Research Letters*, Vol. 121, 19–25, 2024.

[6] Zheng, J., C. Peng, K. Zhao, and M. Lyu, "A low common-mode SVPWM for two-level three-phase voltage source inverters," *Energies*, Vol. 16, No. 21, 7294, 2023.

[7] Azgın, I., A. Inan, S. Çeliktas, K. B. Acar, M. C. Taplamacioglu, and M. Demirci, "EMI filter design with passive components for power lines," in *2022 International Congress on Human-Computer Interaction, Optimization and Robotic Applications (HORA)*, 1–6, Ankara, Turkey, Jun. 2022.

[8] Zhai, L., G. Hu, M. Lv, T. Zhang, and R. Hou, "Comparison of two design methods of EMI filter for high voltage power supply in DC-DC converter of electric vehicle," *IEEE Access*, Vol. 8, 66 564–66 577, 2020.

[9] Ali, M., J. Friebe, and A. Mertens, "Design and optimization of input and output EMI filters under the influence of parasitic couplings," in *2021 23rd European Conference on Power Electronics and Applications (EPE'21 ECCE Europe)*, 1–10, Ghent, Belgium, Sep. 2021.

[10] Jie, H., Z. Zhao, H. Li, C. Wang, Y. Chang, and K. Y. See, "Characterization and circuit modeling of electromagnetic interference filtering chokes in power electronics: A review," *IEEE Transactions on Power Electronics*, Vol. 40, No. 1, 920–943, 2025.

[11] Wu, H., "Analysis and design of insertion loss of EMI filter based on improved differential evolution algorithm," in *2023 International Conference on Applied Intelligence and Sustainable Computing (ICAISC)*, 1–5, Dharwad, India, Jun. 2023.

[12] Yilmaz, Z. S., M. I. Ince, M. S. Ayas, and E. Sag, "Comparative study of GA and PSO algorithms in EMI filter optimization," in *2025 Innovations in Intelligent Systems and Applications Conference (ASYU)*, 1–6, Bursa, Turkiye, Sep. 2025.

[13] Viani, F., F. Robol, M. Salucci, and R. Azaro, "Automatic EMI filter design through particle swarm optimization," *IEEE Transactions on Electromagnetic Compatibility*, Vol. 59, No. 4, 1079–1094, 2017.

[14] Cui, Y., X. Meng, and J. Qiao, "A multi-objective particle swarm optimization algorithm based on two-archive mechanism," *Applied Soft Computing*, Vol. 119, 108532, 2022.

[15] Xu, X.-F., K. Wang, W.-H. Ma, C.-L. Wu, X.-R. Huang, Z.-X. Ma, and Z.-H. Li, "Multi-objective particle swarm optimization algorithm based on multi-strategy improvement for hybrid energy storage optimization configuration," *Renewable Energy*, Vol. 223, 120086, 2024.

[16] Shang, J. and G. Li, "A hybrid composite differential evolution and multiobjective particle swarm optimization evolutionary algorithm and its application," *IEEE Access*, Vol. 12, 74 417–74 431, 2024.

[17] Madani, A., A. Engelbrecht, and B. Ombuki-Berman, "Cooperative coevolutionary multi-guide particle swarm optimization algorithm for large-scale multi-objective optimization problems," *Swarm and Evolutionary Computation*, Vol. 78, 101262, 2023.

[18] CISPR 11:2024, Industrial, scientific and medical equipment — Radio-frequency disturbance characteristics — Limits and methods of measurement.